Manipulation of Atoms by Laser Light

1992 Phys. Scr. 1992 23

(http://iopscience.iop.org/1402-4896/1992/T40/003)

Physica Scripta. Vol. T40, 23–31, 1992.

Manipulation of Atoms by Laser Light

W. Ertmer

Institut für Angewandte Physik, Universität Bonn, Wegelerstr. 8 D-5300 Bonn, FRG

Received November 14, 1991; accepted November 15, 1991

Abstract

Laser cooling and laser manipulation of free neutral atoms have reached a level of sophistication not foreseen just a few years ago. This concerns trapping of neutral atoms at μK temperatures as well as the precise preparation of extreme dense and ultra cold atomic beams. These techniques offer a plenty of new experiments answering basic physical questions or allowing totally new levels of precision. The following article will explain, how to prepare such cold beams and it will demonstrate the resulting possibilities for a Ramseyspectrometer at the intercombination line of Magnesium. Furthermore first results with this spectrometer set up as Magnesium atom-interferometer will be presented.

1. Introduction

During the recent past various methods have been developed to cool and to manipulate the motion of free atoms by laser induced radiation pressure [1]. These techniques open generally two regimes of manipulation: the confinement of atoms by radiation fields in so called atom traps [2] or optical molasses [3] and the manipulation of atomic beams [4]. In this paper we will discuss several beam preparing methods to achieve very bright, slow and monochromatic atomic beams. This includes the deceleration of an effusive atomic beam, its velocity dependent deflection and its consecutive compression. The techniques described here, especially the atomic beam compression, offer interesting insights in the complex polarization dependent interaction between atoms and more dimensional laser beam configurations [1]. Moreover they provide a powerful tool for the preparation of atomic samples, e.g., in high resolution atomic spectroscopy, quantum optics, surface studies, atomic collisions, investigations of basic quantum phenomena, atomic interferometry and many more applications. The last step, atomic beam compression, will show important differences between "atom optics" and "photon optics".

The achievable high density of atoms at low velocities allows considerable improvements of the resolvable line Q and the signal to noise ratio at narrow transitions. In addition it effectively reduces shifts and broadening effects like the quadratic Doppler effect or transit time broadening.

Thus in the second part of this paper I will present experimental results on laser cooling of Mg and first experiments with the Mg intercombination line. The intercombination line of magnesium $^1S_0$–$^3P_1$ ($\lambda = 457.1$ nm) is an interesting candidate for precision experiments. Mg can be cooled and manipulated by the fast $^1S_0$–$^1P_1$ transition at 285.3 nm. Its intercombination line offers a resolution in the Hz regime according to its small natural linewidth of $\Delta\nu = 35$ Hz ($\tau(^3P_1) = 4.6$ ms [5]). To take advantage of the high Q value ($Q \approx 2 \cdot 10^{13}$) the separated field method, adapted for optical, Doppler free experiments [6, 7] may be used. In this paper we will describe the observation of Ramsey fringes on the intercombination line and first experimental results on atom interferometry using atomic inner state labeling.

2. Manipulation of atomic beams

2.1. *Preparation of slow atoms*

In principle there do exist two methods to produce slow atomic beams: very slow beams have been generated from ensembles of trapped atoms by launching the atoms or parts of the ensemble by laser light to form an atomic fountain [8]. These atoms have an average velocity of less than a few m/s, but the density of such a fountain beam is typically fairly low. Thus for various applications it may be easier or better suited to work with a beam of at least a few 10 m/s, e.g., to maintain a low divergence.

Such slow beams are generally prepared from effusive thermal atomic beams, which are decelerated by the radiation pressure force of a counterpropagating laser beam. Several methods have been well established for this purpose [9]. They differ mainly in the solution of two generic problems occurring in such cooling experiments: optical pumping and keeping the resonance condition between the decelerating laser beam and the fast changing Doppler shift of the down slowing atoms [9].

The experiments described here start with laser cooling of a sodium atomic beam as the first step, using the frequency chirp method [10]. The general experimental result (as for the other deceleration methods [9, 11], too) is an atomic beam with a strongly modified velocity distribution: it contains a major cold and slow part with a longitudinal velocity spread of typically a few m/s, corresponding to a temperature T of $T < 30$ mK. But the total atomic beam is not yet monoenergetic, because it still contains the unaffected high-velocity wing of the Maxwell-Boltzmann distribution. In addition the strong cooling laser light is still superimposed and the transverse beam temperature of the laser cooled atoms is enlarged by diffusion processes caused by the numerous recoils as consequence of the spontaneously emitted photons during deceleration.

Therefore the separation of the laser cooled atoms from the residual atomic beam by velocity selective laser deflection may be the right tool to generate a really monoenergetic, slow atomic beam, undisturbed by strong laser light.

2.2. *Atomic beam deflection*

If the prepared atomic beam is crossed perpendicularly by a near resonant laser beam, all the crossing atoms will gain transverse momentum in the direction of the deflecting laser

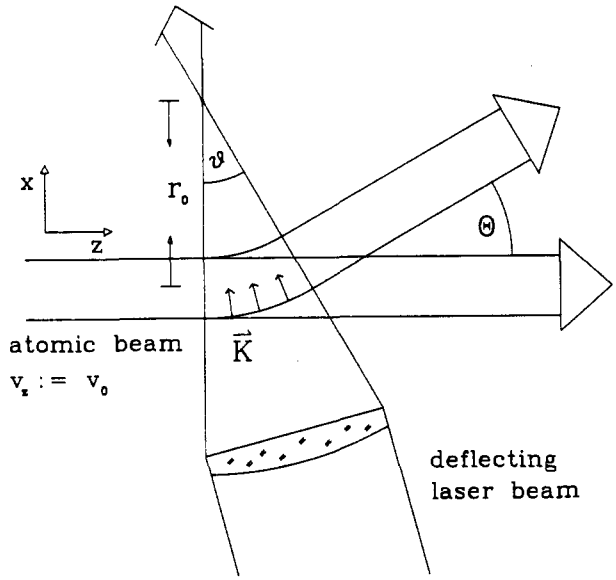

Fig. 1. Principle scheme of laser deflection

beam because of the Doppler free geometry. The resulting deflection angle depends as well on the interaction time as on the longitudinal velocity. Thus the deflection angle depends nearly quadratically on the atomic longitudinal velocity.

The easiest apparative arrangement for deflection would be a transverse (Gaußian) plane wave running perpendicularly to the atomic beam axis [12]. But because of the acceleration in the direction of the transverse laser beam the atoms are Doppler shifted out of resonance thus limiting the deflection angle to typically less than 10° for 100 m/s sodium atoms [12]. The resulting transverse velocity width and hence the divergence is governed mainly by the velocity dispersion of the deflection mechanism of the plane wave as well as by the (limited) cooling action of the fixed frequency laser in the plane of deflection.

Figure 1 shows an improved geometry for atomic beam deflection avoiding these disadvantages [13]. The arrangement of the light field propagating always perpendicularly to the atomic trajectories permits a stabilization of the resulting atomic orbits by detuning locking [13]. The competition between the centrifugal force and the strongly direction-dependant light pressure force can lead to a damping of the transverse velocities in the plane of deflection up to the Doppler-limit [14] $T \approx \hbar\Gamma/2k_B$ ($\Gamma = 1/\tau$, τ: nat. life time of the upper cooling transition) of $T \approx 240\,\mu$K for sodium (in the limit of a two-level system). For the desired circular orbit ($\boldsymbol{k} \perp \boldsymbol{v}$), the angle of deflection Θ equals the angle δ between the marginal rays of the deflecting light field. If this light field is formed by a cylindrical lens the intensity distribution $I(r)$ becomes proportional to $1/r$ and thus the angle of deflection becomes independent of radius r (for saturation $s \ll 1$). The details of the deflection mechanism are given in Ref. [13].

Figure 2 sketches the experimental setup. It shows the atomic beam and the counterpropagating cooling laser beam, part of which is split off behind the first electrooptic modulater (EOM1) as deflecting laser beam. The cooling laser is tuned half a linewidth below resonance to match optimum deflection efficiency [13]. The first electrooptic modulator generates repumping sidebands to compensate for optical pumping during the deceleration [10] and the deflection process. Owing to the chirp method the fast swept sidebands in the slowing laser beam are produced by a second electrooptic modulator (EOM 2). A second dye laser was used as probe laser; its beam crossed the atomic beam axis 25 cm downstream of the deflection zone (point A in Fig. 2). To measure the angle of deflection as well as the profile of the deflected atomic beam a photomultiplier (PM) was located 25 cm downstream of the deflection zone moveable in the direction of the probe laser beam (point B in Fig. 2).

Figure 3 shows some typical velocity distributions in the undeflected (point A in Fig. 3) as well as in the deflected atomic beam (point B); the deflection angle was set to 30°. Figure 3(a) and (b) show the velocity distribution of the laser cooled atomic beam with (a) and without (b) deflection laser. Figure 3(c) and (d) show the (transverse) velocity distribution at point B with and without laser cooling. Figure 3(c) demonstrates, that there are nearly no slow atoms (which would have been deflected too) in the thermal atomic

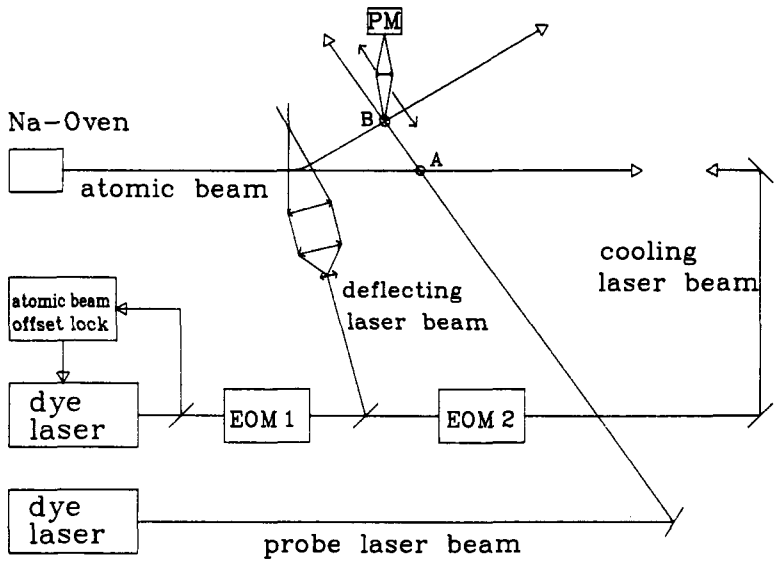

Fig. 2. Schematic of the experimental setup for atomic beam deflection

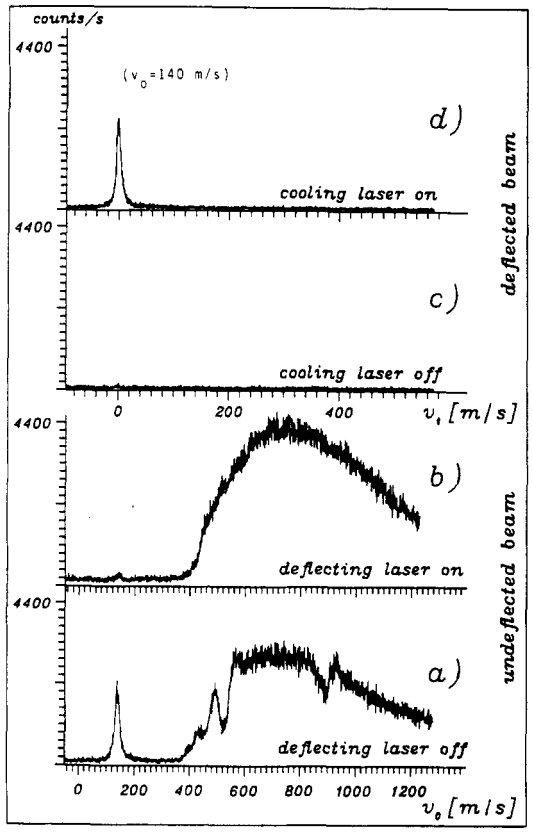

Fig. 3. Typical velocity distributions in the undeflected (a), (b) and deflected (c), (d) atomic beams ($\Delta\nu = -4\,\mathrm{MHz}$, $P_0 = 20\,\mathrm{mW}$ for the $F = 2 \rightarrow F = 3$ transition).

beam, whereas Fig. 3(d) proves the high efficiency ($\approx 100\%$) of the deflection scheme.

The photograph in Fig. 4 shows a top view of the deflection zone with the fluorescence emitted during the deflection process. It demonstrates the nearly circular atomic path inside the deflecting light field. Figure 5 gives the transverse profile of the deflected atomic beam as function of the longitudinal velocity in the deflected beam at point B (Fig. 3). The density in the deflected beam starts with typically 10^6 cold atoms/cm^3 within a diameter of several millimeters, depending on the longitudinal mean velocity, which ranged from 30 to 200 m/s.

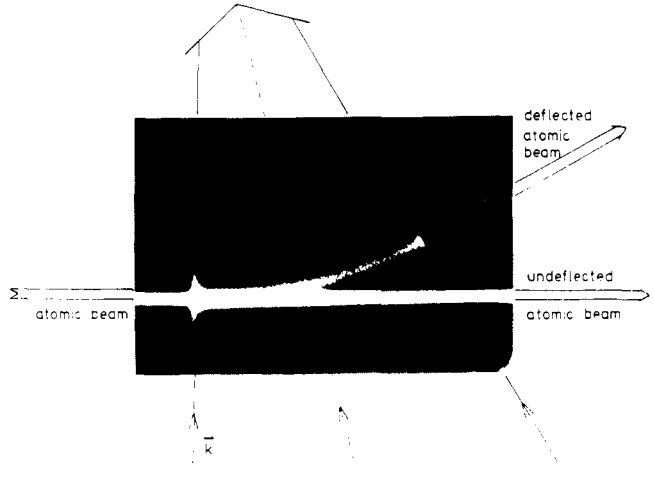

Fig. 4. Photograph (top view) of the deflection zone. The resonance fluorescence of the deflected atoms induced by the deflecting laser shows the circular path of the atoms in the light field

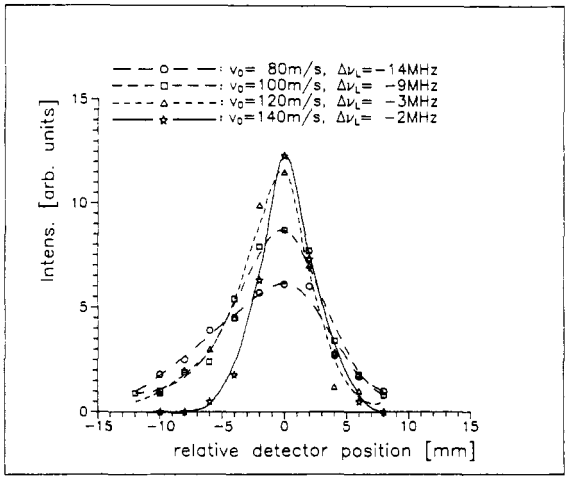

Fig. 5. Measured beam profiles in the plane of deflection. The width corresponds to a transverse temperature of approximately fourtimes the Doppler-limit temperature ($P_0 = 23\,\mathrm{mW}$ for the $F = 2 \rightarrow F = 3$ transition). On this scale, the relative position of the undeflected beam is $-122\,\mathrm{mm}$

Many applications of cold beams, however, will tremendously be improved by higher densities and a reduced diameter of the cold beam. The latest development, discussed in the next chapter, is based on a new two-dimensional magneto-optical arrangement to decrease the beam diameter by two orders of magnitude or more to increase at the same instance the beam density over four orders of magnitude; simultaneously the collimation is kept within the Doppler limit or even better.

2.3. *Magneto-optical compression*

For the compression of an atomic beam in phase space, it is rather advantageous to use the 2-dimensional version of a neutral atom trap. Among various schemes developed and realized up to now, the magneto-optical trap [2, 15] exhibits the deepest potential, exploiting the strong radiative force in combination with the selection rules for radiative transitions between Zeeman-shifted levels of atoms in an inhomogeneous magnetic field.

The principle of operation may be explained for a hypothetical atom with a $J = 0 \rightarrow J = 1$ transition for compression. Two counterpropagating laser beams along x with different circular polarizations are directed towards the axis of symmetry $0z$. A superimposed magnetic field along x, ($\boldsymbol{B} \| \boldsymbol{x}$) with a linearly increasing field strength along x leads to a correspondingly varying Zeeman shift of the level energies. In case of negative laser detuning, an atom at rest will absorb more photons from the laser, which is directed towards the axis, than from the counterpropagating one. In the configuration given, the net force arises from the difference of absorption probabilities from either laser beam, depending on the actual atomic position (magnetic field strength), atomic velocity, laser frequency detuning and magnetic field gradient $\partial B/\partial x$.

For each position x there exists a velocity $v = -\lambda \cdot \mu_B/h \cdot \partial B/\partial x \cdot x$ towards the axis, for which the forces are balanced. As a consequence, the atom will approach the axis like an overdamped harmonic oscillator [2]; for small displacements and velocities the sum of the two radiation pres-

sure forces may be written as:

$$F \approx -\alpha v - m\omega_0^2$$

with

$$\alpha = -\frac{\partial F}{\partial v}, \quad \omega_0^2 = -\frac{1}{m}\frac{\partial F}{\partial x}$$

For sodium atoms and a typical experimental situation ($\partial B/\partial x = 50\,\mathrm{G/cm}$, laser detuning $\delta_L = -7.5\,\mathrm{MHz}$, saturation = 0.75) α/m reads $7.4 \cdot 10^4\,\mathrm{s}^{-1}$ and ω_0 reads $1.75 \cdot 10^4\,\mathrm{s}^{-1}$.

The minimum transverse temperature of the confined atomic beam ($T = m\langle v^2\rangle/k_B$) results in $T \approx \hbar\Gamma/2k_B$, the usual Doppler limit. The final extension $\langle x^2\rangle$, depending strongly on the magnetic field gradient, reads $\langle x^2\rangle = \langle v^2\rangle/\omega_0^2$ (this simple picture holds for small detunings (less than γ) and "two-level configurations" only!).

The force profile (for zero transverse velocity) along x is shown in Fig. 6, emphasizing the influence of the field gradients $\partial B/\partial x$. It reveals that one has to compromise between a large "capture range" (small gradient $\partial B/\partial x$) or a strong restoring force near the axis (strong gradient $\partial B/\partial x$), leading to a minimum excursion of the transversely confined atomic beam. Furthermore, the strongly overdamped harmonic oscillator force, corresponding to a constant gradient $\partial B/\partial x$ along z, seems to limit the achievable "compression factor" [15].

Both difficulties can easily be overcome exploiting the longitudinal motion of the atoms in a magnetic field with an increasing transverse gradient along the z-axis, $\partial B/\partial x(z)$. For slow monoenergetic atomic beams with mean velocities ranging from 30 to 200 m/s, a field gradient increasing from e.g. 50 to 500 G/cm along a z-distance of 40 mm allows a capture range of about 3 mm and an expected final beam diameter of a few μm for a V-level atom. For an increase of the gradient, adapted to the longitudinal velocity, the atom may even experience a constant force along its trajectory, like in laser cooling with a tapered magnetic field [11].

The simplifying V-level treatment may be useful to gain insight in the main aspects of the compression mechanism. For a serious estimate of the final beam diameter or temperature, however, the multilevel structure of the sodium D_2-transition has to be considered, as strong optical pumping between the Zeeman sublevels and the hyperfine levels is expected. To compensate for optical pumping into the $F = 1$ ground state via the $F' = 2$ excited level, we use an additional laser frequency in the compressing beams to repump atoms from the $F = 1$ ground state (see below). As we observe no further compression for increasing repumping laser power in the experiment, we may neglect this kind of hyperfine pumping.

To estimate the influence of optical pumping effects between different magnetic sublevels, a probabilistic approach neglecting induced coherences between the Zeeman sublevels may be a first model. The magnetic quantum number of the ground state is thus treated as a variable subject to random changes $\Delta m_F = \pm 1, 0$, the probabilities of which depend on m_F and Δm_F via the saturations and Clebsch–Gordan-coefficients. The symmetry of the quadrupole field around 0z allows a 1D calculation for the transverse motion, the axis of quantization being always selected along the magnetic field. The additional pair of laser beams in the real two-dimensional experiment is taken into account by their respective portions of σ^+-, σ^-- and π-polarizations and the resulting possible transitions. This modifies the compression process essentially by depopulating the $m_F = \pm F$ states continuously.

The experimental setup, starting from the one described above, is shown in Fig. 7. One of two dye lasers, operating at 589 nm and pumped by one Ar-Ion laser, served as the preparation laser (decelerating and deflecting). The deflecting laser beam, also carrying the repumping sideband, was expanded by a cylindrical telescope and fed through a cylindrical lens to form the deflecting light field. To allow full observation of the compressed beam, the angle of deflection was chosen to be 22° with respect to constraints due to the vacuum chamber.

The second dye laser served as the compression laser. The compression laser was fed through EOM-1, too, to carry the repumping sideband (the repumping intensity being 50% of the carrier intensity); this beam was coupled into an optical single-mode fiber acting as vacuum feedthrough. In addition, the fiber permitted an easy control of the state of polarization inside the magneto-optical molasses (MOM) by use of a simple fiber polarization controller [16]. Inside the vacuum chamber, an output coupler and cylindrical beam

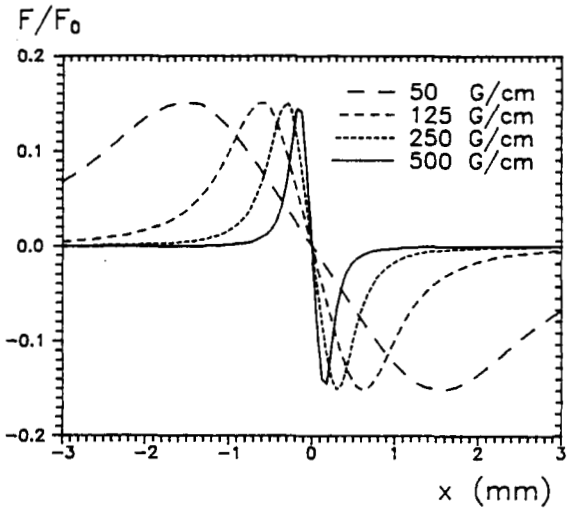

Fig. 6. Net force F in units of $F_0 = \hbar k/2\tau$ for different magnetic field gradients as function of the displacement x (zero atomic velocity assumed)

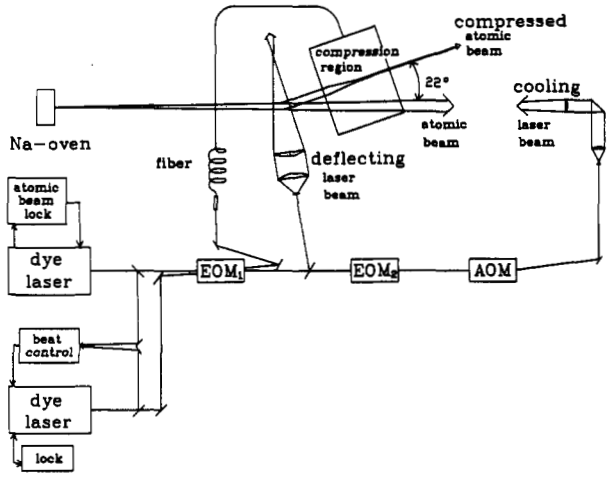

Fig. 7. Experimental scheme for atomic beam compression

expander formed a rectangularly apertured laser beam (50×9 mm) with $w_{0z} = 36$ mm and $w_{0y} = 2.4$ mm. Figure 8(a) shows the deflection region and the compression zone. Downstream the compression zone, the transverse laser beams were linearly polarized and the magnetic fields were shielded. The purely optical molasses formed by these beams preserved the collimation achieved by the MOM. Figure 8(b) shows the optical arrangement forming the four molasses beams.

For the necessary field gradients increasing from 50 G/cm to 500 G/cm, we used 8 small and rather weak (2.1 kG) permanent magnets, which were cut and arranged as shown in Fig. 8(b), to form the linear quadrupole field. The magnetic field was calculated by numerical integration to optimize the shape of the magnets.

The shrinking shape and the resulting diameter of the atomic beam inside the compression region were measured by recording the fluorescence profile either photographically (in 2D) or with an intensified CCD-array aligned perpendicularly to the atomic beam axis. The fluorescence profile was imaged onto the array by a macroscope (outside the vacuum chamber) enabling observation with a magnification of 16 at a distance of 18 cm between front lens and atomic beam. Thus the spatial resolution was about 5 μm. The detector head was controlled by a computer enabling data averaging and background subtraction.

As the atoms are forced towards the axis and the density increases by a factor of several thousand, the beam becomes clearly visible. Downstream, the beam appears as a thin "needle" of constant diameter and brightness. As an example for the measurements with the linear detector, Fig. 9 shows some typical beam profiles for varying longitudinal atomic mean velocities. The position of the detection region was about 27 mm apart from the entrance region, corresponding to a transverse field gradient of 500 G/cm. For atoms moving in a harmonic potential which beomes steeper along their longitudinal direction of propagation, the transverse excursion is expected to depend on the longitudinal velocity. Thus the atomic beam became taller and brighter for decreasing longitudinal velocity. For the velocities under study, the number of slow and compressed atoms, however, remained nearly constant for different longitudinal velocities and furthermore did not undergo any losses along the compression zone. On the other hand, for very low velocities, the incoming beam intensity decreased because of the increasing influence of laser frequency and intensity fluctuations on the photodeflection mechanism [13].

To evaluate the atomic beam diameter, Gaußian distributions were fitted to the data, the result of which are shown in Fig. 9. For atoms with $v_z = 47$ m/s the beam diameter is less than 50 μm. For atoms slower than 40 m/s, the transverse acceptance of the MOM (in the momentary version) is not adapted to the incoming deflected beam. The frequency of the compression laser was $\nu_0 - 7$ MHz, the laser power in the MOM (all sidebands) was 20 mW.

The new method of simultaneous focussing and collimation of slow atomic beams, as described here, has successfully been tested experimentally with a laser cooled

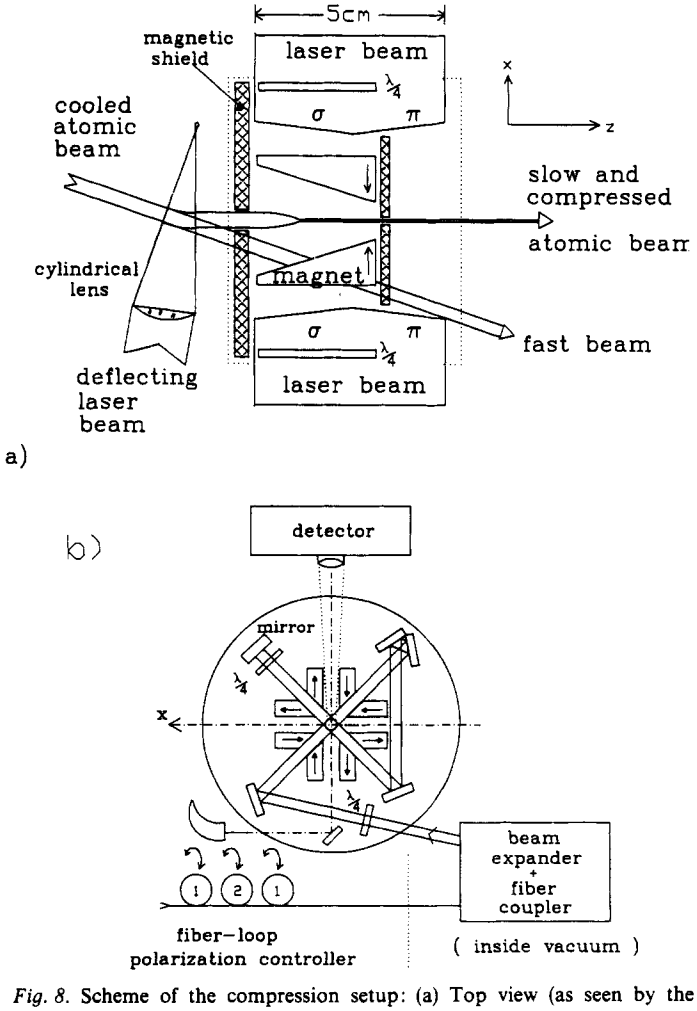

Fig. 8. Scheme of the compression setup: (a) Top view (as seen by the detection system), (b) view in a plane perpendicular to the atomic beam

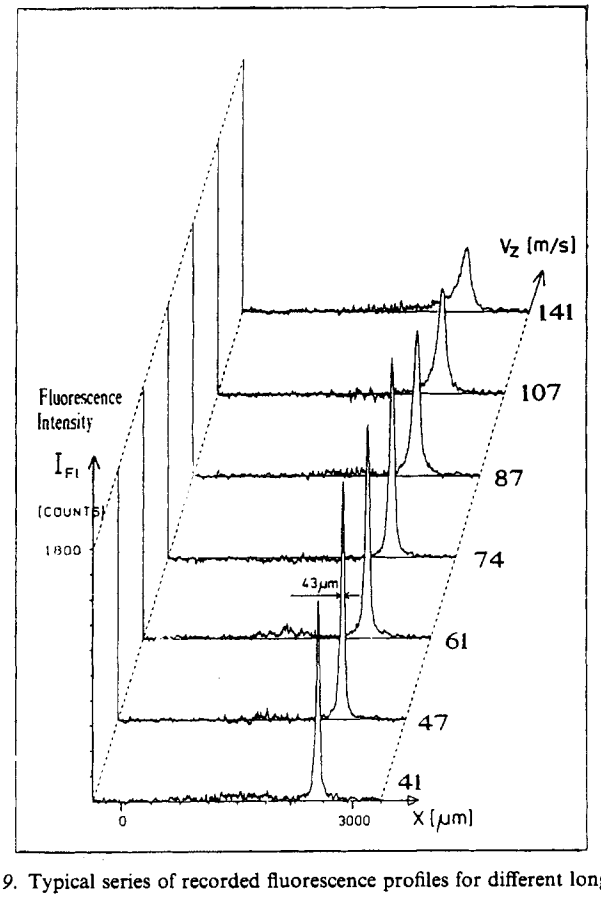

Fig. 9. Typical series of recorded fluorescence profiles for different longitudinal velocities v_z. The detector was located at $z = 30$ mm

sodium beam to reduce the diameter of the monoenergetic (50 m/s) beam from several millimeters down to 43 μm. This boosted the density by more than three orders of magnitude to approximately 10^9–10^{10} cold atoms/cm^3. This density can easily be improved by an increase of the incoming cold beam density from 10^6/cm^3 to 10^8/cm^3 gaining 10^{11}–10^{12} cold atoms/cm^3 at 50 m/s within a 40 μm beam. The final diameter, depending strongly on the magnetic field gradient, can easily be further decreased within the given length of the interaction zone by simply using stronger magnets. Atomic beams, as described here, are very valuable sources for many interesting experiments as e.g. collision experiments or atomic interferometers, which demand precise control of the atomic motion as well as a maximum intensity of the ultracold atomic beam.

The small final diameter would also enable further focussing by the dipole force using an axicon mirror [17] or similar arrangements overcoming the relatively small spatial "capture range" of those schemes. Thus cold atomic beam diameters in the range of λ become accessible [4]. The compression could be seriously increased by transverse "sub-Doppler-molasses" or "sub-Doppler magnetooptical molasses" setups using polarization gradient cooling [18]. The real further decrease in phase space volume, which might be expected from such schemes, however, is difficult to predict: It is essential to investigate, in how far collective effects as observed in a neutral atom trap [19] limit the density of such a sample of atoms. The interaction between the atoms in the beam due to their radiation fields can be investigated, however, by controlling the flux of atoms fed inside the compression region and observing the resulting beam diameter.

3. Ramsey-interferometer of Magnesium

3.1. *Laser cooling of Magnesium*

Fortunately the Mg atom offers a fast optical transition ($^1S_0 \leftrightarrow {}^1P_1$, $\lambda = 285.2$ nm, $\tau = 2$ ns, $\delta\nu = 79$ MHz) suitable for cooling, manipulating and trapping (see Fig. 10). For ^{24}Mg ($I = 0$) this transition starts from a nondegenerate ground state with no hyperfine splitting so that no optical pumping occurs. In this case laser cooling should be limited by the Doppler limit $k_B T = \hbar\gamma/2$ corresponding to a velocity spread of $v_{rms} = 0.8$ m/s. For ^{25}Mg ($I = \frac{5}{2}$) no optical pumping occurs either, because the hyperfine splitting of the excited state and the Zeeman splitting of the ground level (0.7 kHz/G) are small compared to the linewidth of the transition (79 MHz) even in magnetic fields of some kG. According to this, Doppler cooling works in the same way as for ^{24}Mg, but furthermore sub-Doppler cooling is possible using polarization gradient methods [18].

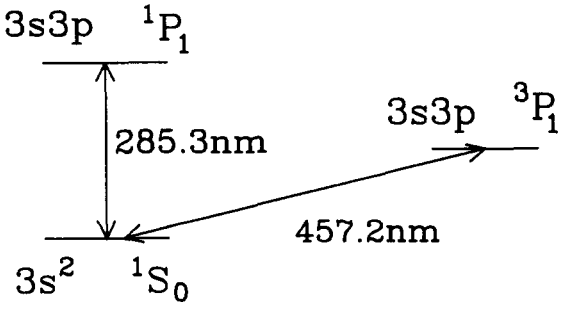

Fig. 10. Energy levels of ^{24}Mg

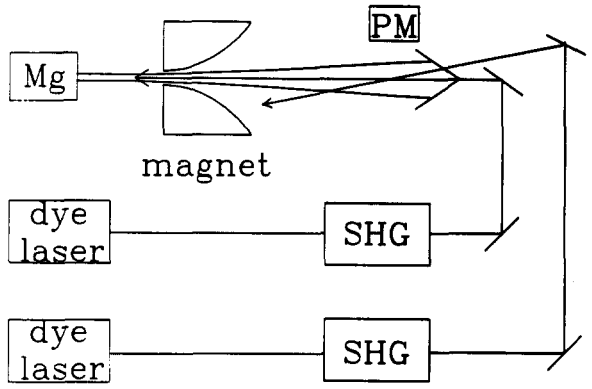

Fig. 11. Laser cooling of a Mg atomic beam: experimental setup

The experimental setup for the cooling experiments is shown in Fig. 11 [20]. A thermal beam of Mg atoms ($T = 730$ K) is decelerated by a counterpropagating laser beam (285.2 nm) within 11 cm and 150 μs, using a tapered permanent magnet to compensate for the varing Doppler shift by Zeeman-shifting the upper level of the atomic transition [11]. For a velocity interval of 1000 m/s corresponding to a Doppler shift of 3.5 GHz a variation of the field by 2.5 kG is required. The 285 nm laser radiation is prepared by second harmonic generation of a 570 nm dye laser beam utilizing noncritical phasematching with ADA in an external cavity. A maximum output power of 30 mW is achieved at 285.2 nm. The velocity distribution of the Mg beam is monitored by the fluorescence induced by a second counterpropagating probe laser beam (Fig. 12). The Mg atoms are decelerated starting at 1000–1200 m/s down to final velocities of 0–200 m/s depending on the cooling laser detuning. The deconvoluted Doppler spectrum yields a velocity spread of the cold Mg atoms of about $\delta v < 10$ m/s corresponding to a temperature of 290 mK. The density is about 10^7 atoms/cm^3 for 100 m/s atoms with a beam radius of 1 mm at the end of the magnet. This cooled atoms will be used in the near future for the high resolution spectroscopic measurements described below.

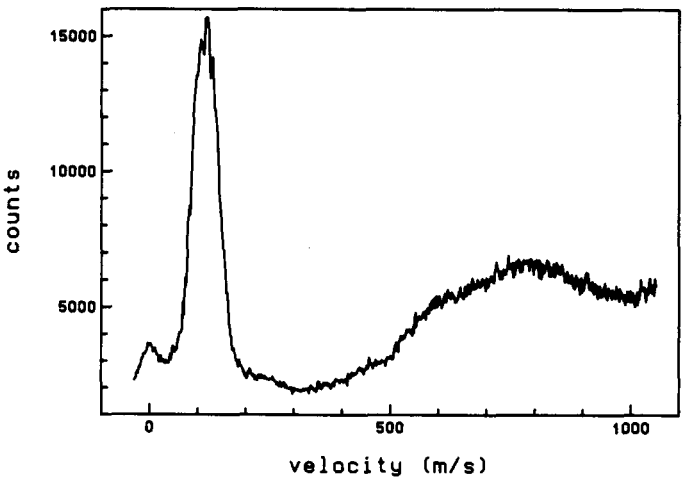

Fig. 12. Measured velocity distribution of a laser cooled ^{24}Mg beam

3.2. *High-resolution spectroscopy of the 457 nm intercombination line*

For the spectroscopic measurements we apply the method of separated field excitation introduced by Ramsey [21] for microwave spectroscopy and transferred to optical frequencies by Bordé *et al.* [6] and Baklanov *et al.* [7]. The experimental scheme is similar to the setup used by Helmcke *et al.* [22] for measurements on Ca. A thermal atomic beam interacts with two equally spaced pairs of copropagating 457 nm laser waves separated by typically $D = 12$ mm (Fig. 13). Nearly perfect retroreflection of the laser beams can be accomplished with two low-aberration lenses and two mirrors in the so-called "cat's eye" configuration. After passing the four laser beams the resulting population in the upper state is monitored by detecting the fluorescence from the decaying $^3P_1$ state 15 cm downstream. To observe the narrow features of the line one necessarily needs a stable laser with high spectral purity. The tunable high resolution laser spectrometer consists of a stilbene 3 dye laser stabilized to the center of a transmission fringe of an ultra-stable nontunable reference cavity by the Pound–Drever method [23]. Tuning of the laser is accomplished by utilizing sidebands generated in an electro-optical modulator with 3 GHz bandwidth. One of the sidebands is stabilized to the center of a transmission fringe of the ultrastable reference resonator. The rms linewidth of the laser is estimated to be 200 Hz in a 10 kHz bandwidth [24]. Figure 14 shows a typial Ramsey pattern with the blue and red recoil components separated by 79 kHz. The frequency resolution (FWHM) of nearly 10 kHz is mainly caused by transit time broadening.

It was pointed out by Bordé [25] in 1989, that the optical Ramsey setup may be interpreted as an atom interferometer. Each interaction region acts as a coherent beam splitter for the atomic wavefunction. The two parts of the wavefunction behind an interaction zone can be labeled by the internal state and the momentum, e.g., $|g, p\rangle$, $|e, p + \hbar k\rangle$. Internal and external labels are directly correlated. This fact provides the possibility to read out the interferometer output simply by monitoring the excited state population behind the last interaction zone, e.g., by detecting the fluorescence. In order to describe the formation of the interference signal Fig. 15 shows possible trajectories for an atom entering the first laser beam in the state $|g, p\rangle$. After averaging over the transverse momentum distribution only the two closed

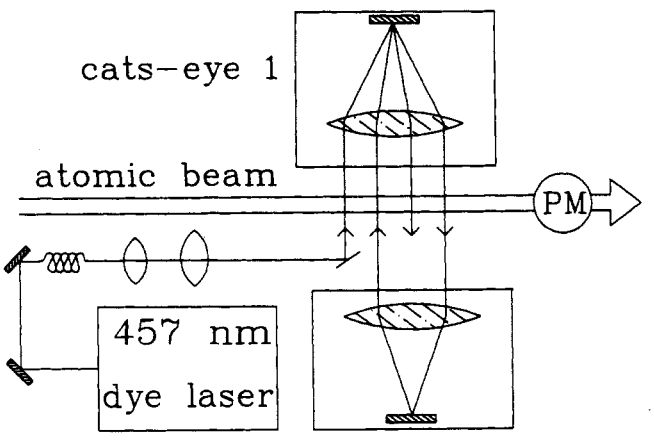

Fig. 13. Optical setup for Ramsey spectroscopy

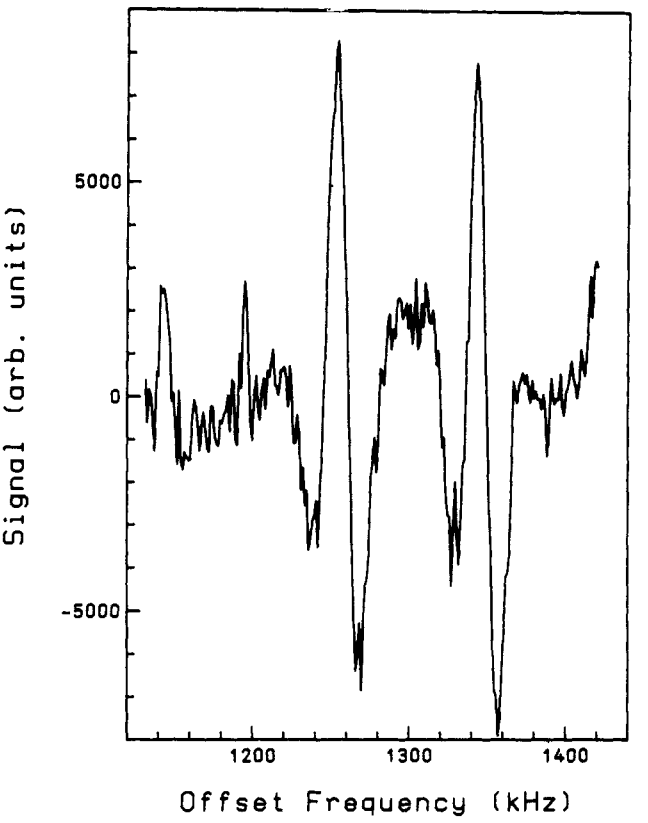

Fig. 14. Observed Ramsey fringes on the $^1S_0 \leftrightarrow {}^3P_1$ transition (Lamb dip background subtracted)

loops shown in Fig. 15 contribute to the Ramsey fringes. Each loop corresponds to one recoil component and represents one complete interferometer. The probability for an atom leaving the last zone in the excited state is proportional to [25]:

$$b_{-1}b^*_{-1} \sim \cos\,[2(\Delta - \delta)T + \Phi_{\text{tot}}]$$

for the blue recoil component and

$$b_{+1}b^*_{+1} \sim \cos\,[2(\Delta + \delta)T + \Phi_{\text{tot}}]$$

for the red recoil component. Here $\Delta = \gamma\omega_L - \omega_0$, $\gamma = (1 - v^2/c^2)^{-1/2}$, $\omega_L/2\pi$ is the laser frequency, $\omega_0/2\pi$ the atom's resonance frequency, $\delta = \hbar k^2/2m$ the recoil shift, $T = D/v$ the transit time, and $\Phi_{\text{tot}} = -\Phi_1 + \Phi_2 - \Phi_3 + \Phi_4$ takes into account the phases of the laser fields.

In the region between the second and the third intraction zone the atoms contributing to the red recoil component are in the excited state $^3P_1$, whereas those contributing to the blue recoil component are in the ground state $^1S_0$. This will allow the suppression of the blue recoil component in a

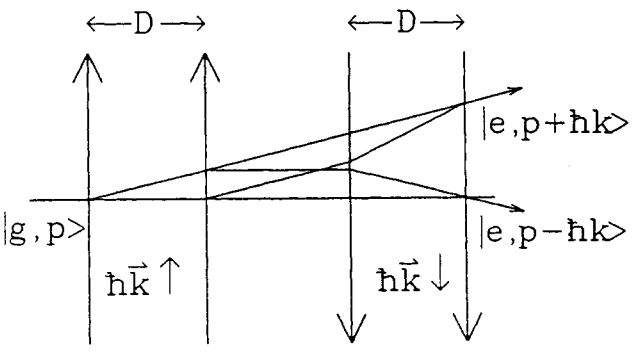

Fig. 15. Atomic trajectories in the Ramsey four-beam interferometer

simple way, if in this region the ground state atoms are excited to the $^1P_1$ state using 285.2 nm laser radiation ($^1S_0 \leftrightarrow {}^1P_1$). Due to the immediately following spontaneous decay the coherence will be destroyed. Furthermore the atoms undergo several absorption-spontaneous-emission cycles in the strong UV beam (15 mW/mm^2) so that they gain considerable transverse momentum. This photo-deflection shifts them out of resonance with the second pair of 457 nm laser beams. In this way also the incoherent "Doppler background" is reduced to 50%. The red recoil component is not affected by the UV beam (Fig. 16).

As in the optical interferometer different interactions in both arms of the matter wave interferometer will lead to an additional phase and thus to a shift of the Ramsey fringes. This can be accomplished for example by the interaction of a potential that acts differently on the two coherent atomic waves. In our experiment this effect of a light shift potential for the ground state atoms on the Ramsey pattern is demonstrated. A 285 nm laser beam (10 mW) tuned several tens of linewidths above the $^2S_0$–$^1P_1$ transition is sent into the region between the third and fourth Ramsey laser beam. The large detuning leads to low excitation and thus to a very small spontaneous emission rate and ensures adiabatic evolution of the atomic state. The potential is given by the dressed atom energy (Fig. 17). For atoms in the $^3P_1$ state no level variation occurs. The additional atomic phase can be calculated by

$$\Phi - \frac{1}{2}\int_0^{T_{UV}} \sqrt{\Delta_{UV}^2 + \Omega^2}\, dt + \frac{1}{2}\int_0^{T_{UV}} \Delta_{UV}\, dt$$

where T_{UV} is the interaction time with the UV laser. For $\Omega \ll \Delta_{UV}$ (Ω: Rabifrequency of the UV-transition) the

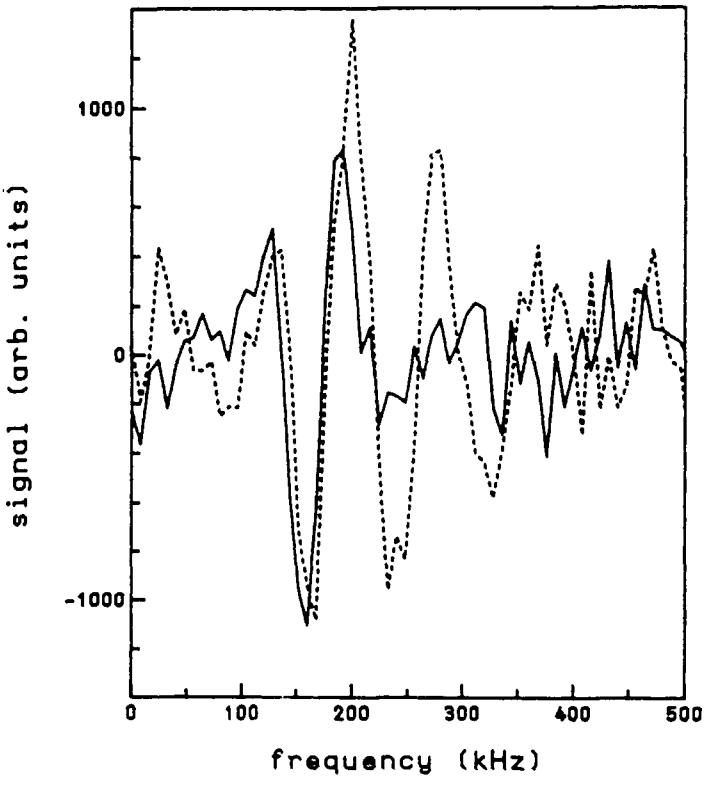

Fig. 16. Suppression of the blue recoil component, solid line: UV-laser on, dashed line: UV-laser off

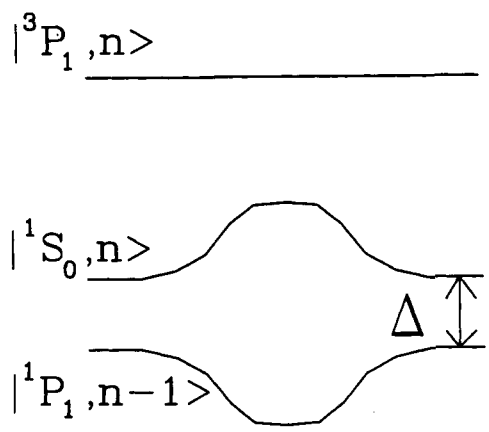

Fig. 17. Spatially dependent AC Stark shift of the $^1S_0$ state induced by the Gaußian laser beam

resulting shift of the Ramsey fringes

$$\Delta = \frac{\Phi}{2T} = -\frac{\Omega^2\sqrt{\pi/2}\, w_0}{4\Delta_{UV}\, 2D}$$

is independent of atomic velocity.

In this experiment with an UV laser beam waist of $w_0 = 1$ mm, $D = 4.9$ mm, a laser power $P_{UV} = 10.5$ mW and a detuning of $\Delta_{UV} = 2\pi(-4\,\text{GHz})$ the calculated shift is $\Delta = 33(5)$ kHz. This agrees very well with the experimentally observed shift (Fig. 18) [26].

Alternatively the fringe shift can be explained by the acceleration of the atom due to the dipole force caused by the crossing UV laser beam. This leads to a time delay of one partial wave [26].

The experiments in the near future will focus on improving the interferometric results using the laser-cooled atoms. To achieve a resolution comparable to the natural linewidth an even more favorable scheme is a pulsed Ramsey experiment with atoms stored and cooled in a magneto-optical trap (Fig. 19). Instead of passing the four travelling waves, the very slow atoms are freely falling from the trap region

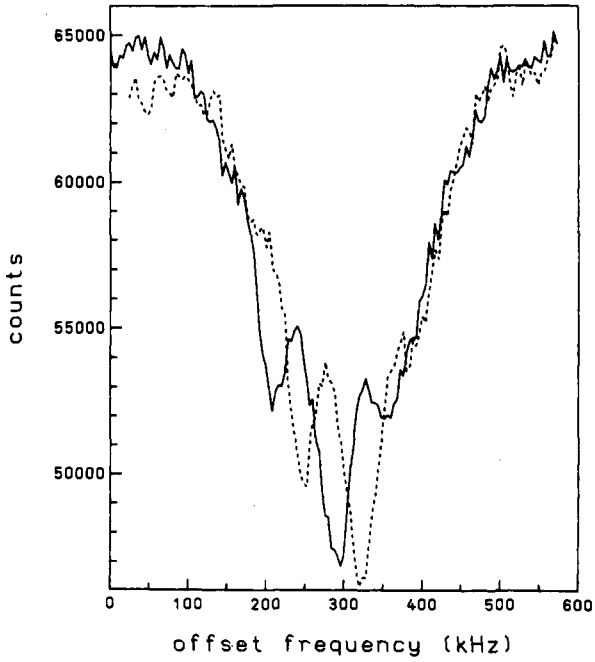

Fig. 18. Observed shift of the Ramsey pattern due to the state selective potential, solid line: UV-laser off, dashed line: UV-laser on

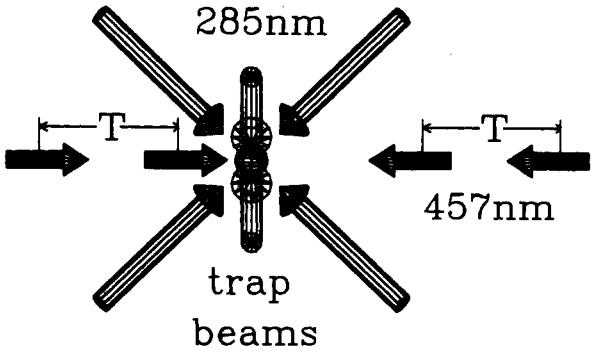

Fig. 19. Scheme of a pulsed Ramsey experiment

and are excited by two counterpropagating pairs of phase coherent 457 nm laser pulses. For a total interaction time of 5 ms a fringe separation of 30 Hz can be expected.

This research was supported by the Deutsche Forschungsgemeinschaft.

References

1. See for example the special issue of J.O.S.A. **B6**, November 1989.
2. Raab, E. L., Prentiss, M., Cable, A., Chu, S. and Pritchard, D. E., Phys. Rev. Lett. **64**, 2631 (1987).
3. Chu, S., Hollberg, L., Bjorkholm, J. E., Cable, A. E. and Ashkin, A., Phys. Rev. Lett. **55**, 48 (1985).
4. Cloppenburg, K., Hennig, G., Mihm, A., Wallis, H. and Ertmer, W., in: "Laser Spectroscopy VIII" (Edited by W. Person and S. Svanberg) (Springer Verlag, Berlin 1987), p. 87.
5. Kwong, H. S., Smith, P. L. and Parkinson, W. H., Phys. Rev. **A25**, 2629 (1982).
6. Baklanov, Ye. V., Dubetsky, B. Ya. and Chebotayev, V. P., Appl. Phys. **9**, 171 (1976).
7. Bordé Ch. J., Salomon Ch., Avrillier, S., van Lerberghe, A., Bréant Ch., Bassi, D. and Scoles, G., Phys. Rev. **A30**, 1836 (1984).
8. Kasevich, M. A., Riis, E., Chu, S. and DeVoe, R., Phys. Rev. Lett. **63**, 612 (1989).
9. See for example the special issue of J.O.S.A. **B2**, November 1989.
10. Ertmer, W., Blatt, R., Hall, J. L. and Zhu, M., Phys. Rev. Lett. **54**, 996 (1985).
11. Phillips, W. D. and Metcalf, H., Phys. Rev. Lett. **48**, 596 (1982).
12. Nellessen, J., Sengstock, K., Müller, J. H. and Ertmer, W., Europhys. Lett., **9**, 133 (1989).
13. Nellessen, J., Müller, J. H., Sengstock, K. and Ertmer, W., J.O.S.A. **B6**, 2149 (1989).
14. Wineland, D. and Itano, W., Phys. Rev. **A20**, 1521 (1979).
15. Nellessen, J., Werner, J. and Ertmer, W., Opt. Comm. **78**, 300 (1990). Riis, E., Weiss, D. S., Moler, K. A. and Chu, S., Phys. Rev. Lett. **64**, 1658 (1990).
16. Lefevre, H. C., Elec. Lett. **16**, 778 (1980).
17. Ertmer, W. and Penselin, S., Metrologia **22**, 195 (1986).
18. Dalibard, J. and Cohen-Tannoudji, C., J.O.S.A. **B6**, 2023 (1989).
19. Walker, T., Sesko, D. and Wieman, C., Phys. Rev. Lett. **64**, 408 (1990).
20. Hennig, G., Bettermann, D., Sengstock, K., Müller, J.-H. and Ertmer, W., to be published
21. Ramsey, N. F., Phys. Rev. **76**, 996 (1949)
22. Helmcke, J., Zevgolis, D. and Yen, B. Ü., Appl. Phys. **B28**, 83 (1982).
23. Drever, R. W. P., Hall, J. L., Kowalski, F. V., Hough, J., Ford, G. M., Munley, A. J. and Ward, H., Appl. Phys. **B31**, 97 (1983).
24. Sterr, U., Sengstock, K., Müller, J.-H. and Ertmer, W., submitted to Phys. Rev. Lett.
25. Bordé, Ch. J., Phys. Lett. **A140**, 10 (1989).
26. Sengstock, K., Müller, J.-H., Sterr, U. and Ertmer, W., to be published